Final Draft
Manuscript available at: https://doi.org/10.1061/(ASCE)BE.1943-5592.0001706
Full citation: Tumbeva, MD, Thrall, AP, and Zoli, TP (2021) "Modular Joint for the Accelerated Fabrication and Erection of Steel Bridges." Journal of Bridge Engineering, 26(6), 04021022

Modular Joint for the Accelerated Fabrication and Erection of Steel Bridges

Mirela D. Tumbeva, S.M.ASCE[1]; Ashley P. Thrall, A.M.ASCE[2]; Theodore P. Zoli, P.E., M.ASCE[3]

ABSTRACT

This paper introduces a new strategy for the accelerated fabrication and erection of steel bridges: a modular joint. The modular joint is a prefabricated, nodal connector comprised of a weldment/built up section of webs and flanges that includes a starter segment for each connecting member. It joins standard rolled wide flange sections through bolted splice connections in double shear. Flanges and webs are connected independently, forming a moment-resisting connection. This provides flexural stiffness for truss-like or beam-like behavior and provides the potential for the structure to tolerate member loss. The flange splice plates connecting the joint and any member can be bent to varying angles to achieve a variable depth geometry. This is a "kit-of-parts" approach, where members are standard sections and the prefabricated modular joint can be repeated throughout a single structure and also used for many structures. While this approach retains all the advantages of modular construction (e.g. prefabrication, mass-production, rapid erection, and reusability), it overcomes the prime deficiency of the existing technologies that a fixed panel size limits the span length. This paper investigates this approach through (1) developing a methodology to achieve rational constant- and variable-depth bridge forms, (2) performing structural optimization for minimum self-weight while meeting structural performance demands and transportability criteria, and (3) demonstrating the promise of this approach through detailed finite element numerical analyses.

[1]Ph.D. Candidate, Kinetic Structures Laboratory, Department of Civil and Environmental Engineering and Earth Sciences, University of Notre Dame, Notre Dame, IN 46556. E-mail: mtumbeva@nd.edu

[2]Myron and Rosemary Noble Associate Professor of Structural Engineering, Kinetic Structures Laboratory, Department of Civil and Environmental Engineering and Earth Sciences, University of Notre Dame, Notre Dame, IN 46556. (corresponding author) E-mail: athrall@nd.edu

[3]National Bridge Chief Engineer, HNTB Corporation, Empire State Building, 350 5th Ave., 57th Floor, New York, NY 10118. E-mail: tzoli@hntb.com

Key Words: Modular construction, Accelerated bridge construction, Steel truss, Optimization

INTRODUCTION

Modular structures (i.e., structures comprised of identical repeated components) provide advantages as components can be prefabricated and mass-produced, resulting in cost and time savings as well as improved quality. These benefits are compounded when the same module can be used for many structures. Existing approaches for modular bridges (e.g., Bailey, Acrow) are comprised of prefabricated, rectangular steel panels [typically 3.05 m (10 ft) in length] that are connected by pins arranged in a longitudinal configuration to form a girder-type bridge, with additional capacity and/or span length achieved by stacking panels transversely and vertically [achieving spans up to approximately 91.4 m (300 ft)] (Figure 1) (Joiner, 2001; Russell and Thrall, 2013). A primary limitation of these existing approaches is that a fixed panel size limits the span length. Specifically, the span is limited by buckling of the upper chord. While lateral bracing can be utilized, it is expensive and can be time-consuming to install (Gerbo et al., 2016a; Wang et al., 2016).

In comparison to girder-type bridges, trusses can be more efficient for longer spans [exceeding 91.4 m (300 ft)]. However, gusset plates are typically used to join members, resulting in the following deficiencies: (1) inefficiency - as bolts are used in single shear, a large number is required leading to increased time and cost of fabrication and erection, as well as reduced net section of the plate, (2) poor durability - as debris can become trapped and connections are subjected to deicing salts, (3) difficult inspection, (4) difficult maintenance as connections are laborious to replace or repair, and (5) challenging fabrication (Covington et al., 2013). These deficiencies have been overcome in the “gussetless” Memorial Bridge connecting Portsmouth, NH and Kittery, ME by using a “knuckle” (Figure 2A). The knuckle enables (1) the use of splice connections in double shear, reducing the number of bolts, (2) the splices to be located away from the concentric intersection of members to facilitate inspection, maintenance, and repair, and (3) the use of wide flange members for the diagonals. The strong axis orientation of the wide flange members and the moment-resisting connections between the members results in increased reliability and redundancy as chords can carry load in bending if a diagonal is lost (Covington et al., 2013). The knuckles are easily fabricated from flat steel plate, with the flanges being cold bent and welded to the webs (Figure 3). Field installation required only bolted connections. This approach offered significant advantages in fabrication and erection time, as well as cost (Covington et al., 2013). The bridge contract was awarded based on a Best Value Award Determination, which included scheduled completion over 4 months faster than competitors, a total project value of $1.1 million less than the next lowest bid, and the highest technical score. This highest technical score was comprised of considerations of aesthetics, maintainability, and long-term durability. As shown in Figure 2, the identical knuckles with curved flange plates and the simple splice connection with fewer fasteners provide a more elegant solution compared to conventional gusset plates. The wide flange members oriented in their strong axis bending gives the bridge a stronger appearance even to the inexperienced eye. The behavior of Memorial Bridge has been studied extensively. Shahsavari et al. (2019) investigated its behavior under live load through field monitoring using accelerometers, uniaxial strain gauges, strain rosettes, and tiltmeters. Chen et al. (2018) measured vibrations on the bridge induced by span lift and traffic loads through camera-based field monitoring. A fatigue evaluation has been conducted by Bell and Medina (2019) through experimentally testing a scaled model of the knuckle subjected to cyclic loads. The results indicated that, with no initial imperfections, an infinite fatigue life is expected. Mashayekhi and Santini-Bell (2019) also investigated the fatigue performance of the knuckle through both field measured data and numerical modeling.

While the “gussetless” Memorial Bridge addressed the deficiencies of trusses, it is not a modular system. It is a one-of-a-kind structure, not a “kit-of-parts” that can be readily adapted for a wide array of spans and loads. The members in the Memorial Bridge were designed to minimize the number of field connections along the span. This resulted in knuckle and chord members (which are built-up steel sections) being fabricated as a single piece, all of which were sufficiently large to require crane erection. In contrast, modular systems should be sufficiently small to fit in shipping containers and to minimize erection equipment requirements. The research in this paper is inspired by Memorial Bridge, but addresses the prime deficiency of that one-of-a-kind structure: that it is not modular.

This research introduces a new strategy for the accelerated fabrication and erection of steel bridges: a modular joint (Figure 4). The modular joint is comprised of a weldment/built up section of web and continuous flanges that includes a starter segment for connection to other modular joints or wide flange structural members. Like the knuckle of Memorial Bridge, the joint can be easily fabricated as the webs and flanges are cut from flat plate. Flanges are cold bent and then welded to the web. Unlike Memorial Bridge, its dimensions are selected for transportability in shipping containers standardized by the International Standard Organization (ISO containers, hereafter). Modular joints can be joined to one another through conventional splice connections to form short-span structures (Figure 5A). Longer spans and increased capacity can be achieved by using standard rolled wide flange members as both the chords and diagonals, all also joined through conventional splice connections (Figure 5B). The wide flange members are easily acquired and only require that holes be drilled. Flanges and webs are connected independently through double shear, bolted splice connections, forming a moment-resisting connection (Figure 6A). This provides flexural stiffness for truss-like or beam-like behavior, providing the potential for the structure to tolerate member loss for enhanced resiliency. Variability in depth (Figure 5C), for improved efficiency or site constraints, is achieved by changing the length of the members and using bent flange splice plates. These bent splice plates can be prebent to a desired angle (e.g., by a press brake) or the adjustable bolted steel plate connection can be used (Figures 6B and 6C).

The adjustable bolted steel plate connection is a slip-critical, angled splice connection comprised of flange plates that are cold bent by press brake to a set of angles. Adjustability is achieved by further cold bending the prebent plates in the field through bolt tightening to achieve the desired angle (Gerbo et al., 2016b, 2018, 2020a,b). The bend radius of the plates (even with field bending via bolt tightening) is required to exceed five times the thickness of the splice plate, in accordance with the current bridge construction code (AASHTO, 2017a). This limit is based on the study by Keating and Christian (2012) which found that strains in plates induced by cold bending should not exceed 10 %, as higher strains would reduce the fracture toughness and ductility of the steel. The service and ultimate (bolt shear failure) behavior of the adjustable bolted steel plate connection was experimentally tested by Gerbo et al (2020b). This research found that the slip and ultimate bolt shear capacity of the adjustable bolted steel plate connection can be reduced (depending on the geometry) due to reduced clamping loads and lack of engagement of shear planes, respectively. Recommendations for the calculation of these reduced capacities were developed. Additional research is necessary for implementation of the adjustable bolted steel plate connection.

The approach proposed in this paper is modular, because identical joints are used repeatedly throughout the structure and among many structures. It is a kit-of-parts - comprised of (1) modular joints that are transportable in an ISO container, (2) standard rolled wide flange sections as both chords and diagonals, and (3) bolted splice connections - that can be used for a wide variety of span lengths and loadings. In comparison to existing modular systems, it can achieve longer spans [targeting 119 m (390 ft)], while providing capability for shorter 39.6-m (130-ft) spans. A more efficient truss topology carries load primarily through axial tension and compression, with the adjustable connection enabling varying depth, to change profile with demand. Bolted splice connections, as opposed to pins, allows for a more durable and reliable connection. The use of double shear connections as opposed to single shear (as is typically used in conventional gusset plates) results in a fewer number of fasteners, thereby reducing assemblage time and facilitating the erection process. This approach also eliminates any field welding thus, saving cost and time. As the modular joint is inspired by the Memorial Bridge, bridges developed using the proposed approach would be able to achieve similar aesthetic qualities. A key aspect to truss performance is joint behavior, and the development of new, more robust joints combined with the principles that have made modular bridges so successful, offers a new paradigm in modular construction: the joint is modularized.

OBJECTIVES AND SCOPE

The objective of this research is to develop a modular joint for the accelerated fabrication and erection of steel bridges and to numerically investigate the behavior of this joint. A methodology is developed to achieve rational constant- and variable-depth bridge forms within the constraints of the developed kit-of-parts. Sizing optimization of the modular joint is performed to minimize the structure self-weight while meeting structural performance demands and transportability criteria. The promise of the modular joint is demonstrated through finite element (FE) numerical analyses. Ultimately, this research presents a fundamentally new approach to, modular construction in which the joint becomes the module and wide flange sections are used to achieve varying structural geometries through bolted splice connections.

DEVELOPMENT OF BRIDGE FORMS

Geometric Parameters of the Modular Joint

To develop a modular joint for both constant- and variable-depth forms, the following geometric parameters are defined (Figure 7): (1) joint length, l, (2) joint angle, θ between the chords and diagonals, (3) depth of the web, h, (4) radii of curvature, R_1 and R_2 of the bent flanges, (5) starter segments lengths, d_1 and d_2, and (6) thickness of the flanges, t_1, t_2, and t_3 and the web, t_4. In this research, it is envisioned that a single modular joint (symmetric about a vertical centerline at point O) would be used throughout a structure and among many structures, to take advantage of cost and time savings of mass producing identical components. However, there could be advantages in considering several versions of the modular joint. For example, smaller and lighter modular joints could be used for shorter span or lower capacity structures. Asymmetric joints or joints with different angles, θ could be considered for different geometries. These are potential areas of future research.

As the geometry is determined such that a single modular joint can be used for many spans, the joint length, l is is chosen to be 3.05 m (10 ft). This is consistent with the length of the panels of existing modular systems, indicating that the joints could be readily handled. The floor beam spacing, for all spans, is also chosen to be this length. For the back-to-back joint layout for short spans, the floor beams would only connect to the modular joints. For longer spans, the lower chord joint spacing is then chosen to be integer multiples of this length, with the floor beams between joints connected to the lower chord. For constant-depth bridges, this is also the upper chord joint spacing. The floor beams which are standard rolled wide flange sections are connected to the lower chord members or lower chord modular joints through web stiffeners using double shear splice plate connections. The bottom flanges of the floor beams are connected to the flat flange of the lower chord modular joints or to the bottom flange of lower chord members through single shear splice plate connections. A lateral bracing system, including portal bracing, also comprised of standard wide flange sections, would be developed for longer span bridges. Lateral bracing would not be provided for the bridge with back-to-back joints layout due to traffic interference. The lateral bracing system is connected to the flat flange of the upper chord joints via plates. Single angle shear connections connect the web of the lateral bracing to web stiffeners (at each upper chord modular joint) as well as to the web of the modular joints. All of these components would be standardized within the kit-of-parts.

The joint angle, θ is chosen to be $60°$ so that the lengths from the center of the joint to the end of each starter segment are equal, ensuring a compact shape for transportation. For longer spans, wide flange members will be utilized between modular joints. As a function of the rolling process, the web depth (i.e., the total section depth minus the thickness of the two flanges) of wide flange sections is approximately the same for sections with the same WXX designation, where XX refers to the nominal depth. This research considers wide flange sections from W14x109 through W14x257 (AISC, 2011), and therefore a joint web depth, h is chosen to be equal to the average web depth of these sections [h = 320 mm (12.6 in.)]. Fill plates could also be used for other section sizes.

The radii of curvature, R_1 and R_2, are both selected to be 508 mm (20 in.). There is an advantage of using larger bend radii as this would increase the overall joint depth and therefore also increase the cross sectional area to transfer the loads from the flange to the web. Furthermore, larger bend radii reduce stress concentrations at welds, making it less sensitive to fatigue (Covington et al., 2013). To satisfy bridge construction code requirements (AASHTO, 2017a) based on limiting residual strains that reduce the fracture toughness and ductility of the steel (Keating and Christian, 2012), the radii must also exceed five times the thickness of the flanges. In this research, Grade 50 structural steel is used for the modular joint. The starter segments lengths, d_1 and d_2 are:

$$d_1 = \frac{l}{2} - \frac{\frac{h}{2} + R_1}{\tan\frac{\theta}{2}}; \qquad d_2 = \frac{l}{2} - \frac{\frac{h}{2} + R_2}{\tan\frac{\theta}{2}} \tag{1}$$

The joint is designed to be nested in ISO containers together with wide flange members, for transportation as shown in Figure 8. Rows of these nested modular joints and members could be arranged on racks that can be offloaded by forklift or other lifting equipment. The ISO container considered for this research has an inner length, E = 12 m (39 ft 4 in.) and inner depth, I = 2.67 m (8 ft 9 in.) (ISO, 2013).

Sizing optimization will be used to determine the thicknesses of the joint flanges and web, as well as the section size of the wide flange members.

Forms for Constant-Depth Bridge

This research develops a "family" of constant-depth simply supported bridges using the modular joint with different spans, S (Figure 9). The focus is on achieving a span of S_1 = 119 m (390 ft) that is the longest in the family and exceeds the span limitations of existing modular systems, while also providing capabilities for shorter spans: S_2 = 79.2 m (260 ft) and S_3 = 39.6 m (130 ft). For each, the joint spacing is bl, where b = number of floor beams between two successive modular joints + 1, as this would facilitate floor beams spaced at a distance, l apart. The depth, D is: $D = \frac{bl}{2}\tan\theta$. For each of these 3 spans, the span-to-depth ratio is 15, which is efficient and economic for truss bridges. The number of modular joints for each is also the same (i.e., 27), such that the kit-of-parts would require the same number of joints regardless of the span. The modular joint would be designed for the highest demand and could then be used for the entire family.

Forms for Variable-Depth Bridges

Variable-depth bridges, in which modular joints are connected to wide flange members at varying angles, γ, can be achieved using conventional bent connections or the adjustable bolted steel plate connection (Figure 5C, 6B and 6C) (Gerbo et al., 2016b, 2018, 2020a,b). This can facilitate more efficient structural forms as depth can be varied with demand and/or accommodate site or architectural constraints. In this configuration, the ends of the members would be cut to the desired angle prior to erection. With the aim of maintaining uniform modular joints throughout the structure, the ends of the starter segments of the joints would not be cut. Thus, a uniform gap between members and joints can be achieved without sacrificing modularity (Figure 6B).

This research proposes a methodology for developing variable-depth bridges based on a structural performance metric for a given (1) span length, S, (2) span type (i.e., simply supported or three-span continuous), and (3) desired variable-depth shape with a prescribed depth, D at the abutments. For varying values of peak depth, H (at midspan for the simply supported, at the interior supports for the continuous) and largest magnitude of angle between components, γ_{max}, the desired variable-depth shape is defined, the coordinates of the modular joints are found, and the structural performance metric is evaluated. The methodology develops a set of solutions for which the structural performance can be readily compared and a designer can select a variable-depth form. This methodology determines the angles between the modular joints and the members, γ, as well as the length of the members.

The following formulation assumes through-type bridges with variable depth upper chords and lateral bracing provided at each upper chord joint. The lower chord joints are assumed to be flat and spaced at a fixed spacing, bl to be consistent with the uniform floor beam spacing discussed earlier. Other configurations could be considered using an analogous methodology.

The structural performance metric in this research is related to reducing the susceptibility to member buckling of upper chord, lower chord, or diagonals members that are in compression under any of the load cases considered. This metric was chosen as member buckling is a major factor in the design of truss bridges. This is quantified as the highest magnitude FL^2 (related to Euler buckling) for any compressive member in the structure, where F is the force in the member calculated using the direct stiffness method (DSM) and L is the unbraced length of the member. Analysis using the DSM models the members as two-node frame elements that are moment-connected (as the modular joint can carry flexure). The modular joints are not modeled explicitly. The unbraced length, L used in this metric is the length of the frame element connecting the center points O of the two joints, as it is assumed that lateral bracing or floor beams will be provided at each joint. The kinks formed between the modular joint and wide flange members were not considered. The effect of the kinks on behavior could be evaluated through high-fidelity numerical models, which would be time-consuming to build and analyze for a large number of considered geometries. The focus of this paper is on developing a quick and computationally inexpensive way to compare the behavior of many different bridge forms. A uniform section size for all members was assumed (i.e., W14x109) for simplicity. The load includes self-weight of the upper chord, lower chord, and diagonal members (applied as uniformly distributed load along each member, neglecting the joints for simplicity), self-weight of a lightweight deck of 1.2 kN/m^2 (25 psf), and two lanes of vehicular traffic represented by two design lane loads from the bridge design code [18.7 kN/m (1.28 kips/ft) in total (AASHTO, 2017b)]. The live load and the load from the lightweight deck are applied as a uniformly distributed load at the lower chord along the entire span, as the floor beams are connected to the lower chord members at every l = 3.05 m (10 ft) in the longitudinal direction. Note that this is different from typical trusses where the load is transferred only at the nodes. Only one plane of the bridge is modeled. For the simply supported bridge, the boundary conditions are: at one end, free rotation about the transverse axis, translation restrained in longitudinal and vertical directions; at the other end, free rotation about the transverse axis, free translation along the longitudinal axis, and translation restrained in the vertical direction. For the continuous bridge, the boundary conditions are: at one of the abutments, free rotation about the transverse axis, translation restrained in longitudinal and vertical directions; at the piers and the other abutment, free rotation about the transverse axis, free translation along the longitudinal axis, and translation restrained in the vertical directions. When comparing different bridge forms, the bridge with the lowest value of the structural performance metric would have the lowest susceptibility to member buckling and would, therefore, be preferred. Other performance metrics could be considered. This research selects the structural performance metric, FL^2, as it allows the methodology to rapidly search the design space for finding a bridge form with an enhanced member buckling capacity.

To achieve the variability in depth, this research utilizes the adjustable bolted steel plate connection. The connection is comprised of $10°$, $20°$, and $30°$ prebent flange plates, as well as flat plates, that can be further bent in the field through bolt tightening to achieve the desired angles. To limit the strains induced in the bolts during field installation, the amount of field bending should be limited to $\pm 5°$ (Gerbo et al., 2018, 2020a,b). As only angle changes up to γ = $35°$ were investigated, this research considers angle changes, γ between components up to this value. As there are benefits in smaller angles and in using flat plates that are field-bent only, this research considers differing values of the largest magnitude of allowed angle, γ_{max}. Conventional, bent splice plate connections could alternatively be used.

The desired variable-depth shape of each bridge can be defined based on structural demands, site constraints, or other priorities. In this paper, the desired shape for the simply supported bridge is a parabola, with a depth, D at the abutments and a depth, H at midspan ($H > D$), to approximate the bending moment diagram of a simply supported beam under uniformly distributed load. For the three-span continuous bridge, the desired shape in this research relates to the envelope of the moment diagram with a uniformly distributed load over: (1) the entire bridge span, (2) half of the entire bridge, (3) on any of the three spans, and (4) on any of the two spans. For each load, the highest value of the moment is calculated and is scaled to relate to a depth, H at the inner supports. At the abutments, the height is the depth, D.

The coordinates of the upper chord joints, U_i (where the index i is counted from the origin Ω, Figure 10) and the lower chord joints, L_i are found to achieve the variable-depth shape. As shown in Figure 10, the angles between the modular joints and the members, γ_i^1 - γ_i^6 (Table 1), vary to achieve the variable depth form. Specifically, the coordinates of the upper chord joints are found by varying the angles γ_i^1, γ_i^2, and γ_{i-1}^4 between $-\gamma_{max}$ and $+\gamma_{max}$, with increments of $1°$. The value of γ_i^3, γ_i^5, and γ_i^6 are calculated using the equations in Table 1 and discussed later. As the angles vary, thousands of different locations for each upper chord modular joint exist. The permutation of these angles that gives coordinates for each upper chord joint closest to the desired depths, y at a distance, x from the origin Ω are selected. In this methodology, the angles, γ_i^3, γ_i^5, and γ_i^6 are required to be less than or equal to γ_{max} and the length of each upper chord, T_i, diagonal, N_i

and M_i, and lower chord, G_i member is required to be less than the inner length, E of the ISO shipping container (Figure 8). If these criteria are not met for a joint, the permutation of angles is rejected and the next permutation with coordinates closest to the desired shape, that also satisfies the length criteria, is selected. Following this methodology, the coordinates of the upper chord joints are found progressively moving out from the origin to ultimately achieve the desired span length. Both the simply supported and continuous bridges are assumed to be symmetric about their center lines.

Simply Supported Bridges

The coordinates of the joints (where coordinate of a joint refers to the location of the joint center O) for the simply supported bridge are found by beginning with an upper chord joint, U_0 placed at midspan (i.e., x_{U_0} = 0 and y_{U_0} = H), as its corresponding lateral brace would restrain the system against buckling at this location of highest compression (Figure 10A). It is parallel to the lower chord for symmetry. The coordinates of joint L_0 are: x_{L_0} = $bl/2$ and y_{L_0} = 0, with the coordinates of the subsequent lower chord joints L_i (for $i > 0$) being:

$$x_{L_i} = x_{L_{i-1}} + bl \tag{2}$$

$$y_{L_i} = 0 \tag{3}$$

The coordinates of the subsequent upper chord joints U_i (for $i > 0$) are:

$$x_{U_i} = x_{L_{i-1}} + (l/2)\cos\theta + (l/2)\cos(\theta - \gamma_i^1 + \gamma_i^5) + M_i \cos(\theta - \gamma_i^1) \tag{4}$$

$$y_{U_i} = (l/2)\sin\theta + (l/2)\sin(\theta - \gamma_i^1 + \gamma_i^5) + M_i \sin(\theta - \gamma_i^1) \tag{5}$$

where γ_i^1 is varied between $-\gamma_{max}$ and $+\gamma_{max}$ and $\gamma_i^5 = \gamma_i^1 - \alpha_i$. The angle, $\alpha_i = \alpha_{i-1} + \gamma_i^2 + \gamma_{i-1}^4$, is between OA' of joint U_i and a horizontal line passing through the center O of joint U_i. Note that

$\alpha_0 = 0$. Angles γ_i^2 and γ_{i-1}^4 are varied between $-\gamma_{max}$ and $+\gamma_{max}$. M_i is the length of the diagonal member center line and is calculated as follows:

$$M_i = f\frac{\sin\eta}{\sin\psi} - u\frac{\sin\varphi}{\sin\psi} \tag{6}$$

where $f = \sqrt{\Delta e^2 + \Delta v^2}$ with:

$$\Delta e = x_{L_{i-1}} - x_{U_{i-1}} + (l/2)(\cos\theta - \cos\alpha_{i-1}) \tag{7}$$

$$\Delta v = y_{U_{i-1}} - (l/2)(\sin\theta + \sin\alpha_{i-1}) \tag{8}$$

The distance, $u = l\cos\theta$ is determined from triangle $B'O'A'$. The angles are: $\psi = \theta - \gamma_i^1 + \gamma_{i-1}^4 + \alpha_{i-1}$, between the upper chord T_{i-1} and the diagonal M_i, $\eta = \beta - \gamma_{i-1}^4 - \alpha_{i-1}$, between the upper cord T_{i-1} and line CA, and $\varphi = 90 - (\theta/2) + \gamma_i^2$, between $A'P$ and $B'A'$. The angle, $\beta = \arctan(\Delta v/\Delta e)$ is between the horizontal and line CA. Once the coordinates of U_i and L_i are found, the angles γ_i^3 and γ_i^6 need to be calculated to ensure that they are less than γ_{max}:

$$\gamma_i^3 = \gamma_i^6 - \gamma_i^1 + \gamma_i^5 \tag{9}$$

$$\gamma_i^6 = \arctan\left(\frac{y_{U_i} - (l/2)\left[\sin\theta + \sin(\theta + \alpha_i)\right]}{x_{L_i} - x_{U_i} - (l/2)\left[\cos\theta + \cos(\theta + \alpha_i)\right]}\right) - \theta \tag{10}$$

The lengths of each member is calculated to ensure that they are less than E. The upper chord T_{i-1} is:

$$T_{i-1} = f\frac{sin(\psi + \eta)}{\sin\psi} - u\frac{\sin(\psi + \varphi)}{\sin\psi} \tag{11}$$

The lower chord members have a constant length due to fixed lower chord spacing: $G_i = (b-1)l$. The length of the diagonal member M_i is given by Equation 6 and the length of diagonal member N_i is:

$$N_i = \frac{y_{U_i} - (l/2)\left[\sin\theta + \sin(\theta + \alpha_i)\right]}{\sin(\theta + \gamma_i^6)} \tag{12}$$

Because the angles γ must not exceed γ_{max}, there is a limit on the depth at midspan, H_{max} which can be calculated as follows:

$$H_{max} = l \sin\theta + [(bl/2) - l\cos\theta] \tan\left(\theta + \gamma^6_{0,max}\right) \tag{13}$$

where $\gamma^6_{0,max}$ is equal to γ_{max}.

These equations do not account for interference between the joints and members which can be avoided by cutting members or decreasing d_1 and d_2. These equations assume a clockwise angle is negative, and a counterclockwise angle is positive.

Three-span Continuous Bridges

The coordinates of the continuous bridge can be similarly found, with the following differences. A lower chord joint, L_0, is positioned above the first pier, which serves as the origin, Ω (i.e., x_{L_0} = 0; y_{L_0} = 0, Figure 10B). The upper chord, T_0 is centered above this joint and oriented horizontally at the depth, H. Thus, γ^0_4 = 0 and α_0 = 0. The coordinates of the first upper chord joint, U_1 are calculated using Equations 2 through 8, with the exception that for this joint, $\Delta e = (l/2)\cos\theta$ and $\Delta v = H - (l/2)\sin\theta$. The coordinates of the successive modular joints, as well as the equations for the angles, γ and the member lengths, are the same as the prior section.

The limit, H_{max} on the depth at the piers is found by varying the angles γ^1_1, γ^1_2 and γ^1_6 between $-\gamma_{max}$ and γ_{max}. For each permutation of these angles, a depth H_s is calculated: $H_s = y_{U_1} + (l/2)\sin\alpha_1$, where y_{U_1} is calculated using Equation 5 but with M_1 found as follows:

$$M_1 = \frac{(l/2)\tan(\theta+\gamma^1_6)\,[2b - 2\cos\theta - \cos(\theta-\alpha_1) - \cos(\theta+\alpha_1)] + (l/2)\,[\sin(\theta+\alpha_1) - \sin(\theta-\alpha_1)]}{\sin(\theta-\gamma^1_1) + \cos(\theta-\gamma^1_1)\tan(\theta+\gamma^1_6)} \tag{14}$$

Note that Equation 6 cannot be used, as the depth is not yet known. The angles γ^3_1 and γ^5_1 must not exceed γ_{max}. The largest value of H_s will be H_{max}.

Form Comparison

The proposed methodology is implemented for two case studies: a 119-m (390-ft) simply supported bridge and a three-span continuous bridge [101 m (330 ft) - 119 m (390 ft) - 101 m (330 ft) spans]. For both, b = 3, corresponding to a lower chord joint spacing of 9.14 m (30 ft). The depth, D at the abutments is the same depth as the constant-depth 119-m (390-ft) simply supported bridge for comparison [D = 7.92 m (26 ft)]. The depth H varies between D and H_{max} in increments of 0.305 m (1 ft). A comparison of the structural performance metric for varying values of H and γ_{max} are shown in Figure 11. The performance metric for constant-depth forms are also included for comparison.

The developed methodology is a geometric problem coupled with structural performance criteria that develops variable-depth forms within the constraints of the modular joint approach. There is a large number of permutations in the solution space depending on the ranges of the angles γ, number of modular joints along the bridge span, and length of the members. For example, for the constant-depth 119-m (390-ft) simply supported bridge with γ_{max} = 15^o, there are 29,791 possible permutations of the angles for a single upper chord joint. There are six upper chord joints along half of the span resulting in 178,746 permutations that were investigated for a given depth H. For the γ_{max} = 15^o case, there are 22 different values of H resulting in a total of 3,932,412 permutations. The goal of this study was to explore all possible permutations of the angles γ, while limiting the susceptibility of the compressive members to buckling as well as limiting the length of the wide flange members to meet transportation requirements. These criteria also limit the depth of the structure. Deeper bridges have lower peak compressive forces but increased length of the members. The lowest possible span-to-depth ratio is approximately 8.1 calculated based on the highest value of the depth limit, H_{max}. The highest span-to-depth ratio is 15. The resulting range for the span-to-depth ratio is reasonable for truss bridges. This solution space demonstrates the importance of the methodology to be able to quickly select an efficient form.

Figure 11A shows that the lowest value of the structural performance metric for the simply supported bridge corresponds to γ_{max} = 15° and H = 14 m (46 ft), resulting in a span-to-depth ratio of 8.5 (close to the lowest value). The magnitude of FL^2 depends mainly on the term L^2. However, as γ_{max} increases and L^2 increases as a result, the magnitude of FL^2 actually decreases. This is primarily because by using larger angles, deeper bridges are developed resulting in lower peak compressive forces that are found in the upper chord members at midspan. Additionally, the upper chord member lengths are limited by the lower chord joint spacing and have approximately constant length along the span of 9.14 m (30 ft) for different γ_{max}. Only the length of the diagonal members changes substantially as γ_{max} increases. However, these members have very small (close to zero) axial forces which ultimately lowers the magnitude of FL^2. Thus, as expected, deeper bridges are less susceptible to member buckling. The relative difference in FL^2 between the constant-depth bridge and the lowest FL^2 variable-depth bridge is 40$\%$ which shows the value of considering variable-depth forms using the modular joint.

Figure 11B shows that the lowest value of the structural performance metric for the continuous bridge corresponds to γ_{max} = $35°$ and H = 10.7 m (35 ft), resulting in a span-to-depth ratio of 11.1. Here, the magnitude of FL^2 is mostly influenced by the diagonal members at the piers which have significant compressive forces and are also the longest members. As a result, the forms corresponding to the lowest magnitude of FL^2 for each γ_{max} have a high span-to-depth ratio and a depth, H less than 12 m (40 ft). Although, the peak compressive forces are in the lower chord at the piers, their unbraced length is 9.14 m (30 ft) and therefore, did not significantly impact the results. As in the simply supported case, a variable-depth upper chord reduces the magnitude FL^2 compared to the constant-depth bridge. However, the relative difference in FL^2 between the constant-depth bridge and the lowest FL^2 variable-depth bridge is just 18$\%$. This is mostly because the two bridges have similar forms and thus, similar susceptibility to member buckling.

STRUCTURAL OPTIMIZATION

A sizing optimization approach for minimum self weight, with the aim of improving material efficiency and ease of transportation and erection while meeting geometric and structural constraints, is proposed. This is implemented for the two lane, 119-m (390-ft) long constant-depth simply supported bridge, thereby optimizing the joint for the highest demand of the constant-depth forms. The constant-depth (as opposed to variable-depth) bridge is selected as it has higher susceptibility to member buckling and therefore also represents a worst case scenario. The optimization approach could also be used with other span configurations, span lengths, and/or variable depths. Alternatively, this sizing optimization could be formulated as a multi-objective optimization problem that includes both weight and fabrication/erection cost. This is a potential area for future research.

Problem Formulation

The formal sizing optimization problem formulation is as follows:

$$
\begin{aligned}
\underset{\mathbf{t},\mathbf{s}}{\text{minimize}} \quad & \mathrm{W}(\mathbf{t},\mathbf{s}) = aJ(\mathbf{t}) + pV(\mathbf{s}) + rQ(\mathbf{s}) + oZ(\mathbf{s}) \\
\text{such that:} \quad & c_1 = 5t_k - R_k \leq 0; \qquad k = 1,2 \\
& c_2 = 3g + w + \frac{h + t_1 + t_3}{2}(4 + \cos\theta) + \frac{l}{2}\sin\theta - I \leq 0 \\
& c_3 = \sigma - \sigma_N \leq 0; \\
& c_4 = F_D + \xi F_L - \lambda F_L \leq 0; \\
& c_5 = 0.8K_{in} - K_p \leq 0; \\
& c_6 = \tau_m - \tau_n \leq 0; \\
& \mathbf{t} \in \mathbf{S_T}; \qquad \mathbf{S_T} \in [12.7, 15.9, ..., 63.5]\,\mathrm{mm} \\
& \mathbf{s} \in \mathbf{S_B}; \qquad \mathbf{S_B} \in [W14\text{x}109, W14\text{x}120, ..., W14\text{x}257]
\end{aligned}
\tag{15}
$$

The design variables, $\mathbf{t}$ refer to the thickness of the bent flange plates, t_1 and t_2, flat flange plate, t_3, and web plate, t_4 (Figure 7), which are selected from a discrete set, $\mathbf{S_T}$ in the range between 12.7 mm (0.5 in.) and 63.5 mm (2.5 in.) with an increment of 3.175 mm (0.125 in.). All joints are assumed to be the same. The design variables, s refer to lower chord, upper chord, and diagonal member section sizes, s_1, s_2, and s_3, respectively, which are selected from a discrete set, $\mathbf{S_B}$ of ten different W14 standard wide flange sections in the range between W14x109 and W14x257 (AISC, 2011). Each member type is assigned the same design variable to simplify fabrication and erection (e.g., all upper chords are one section).

The objective function is to minimize the self-weight, W which is the summation of the weight of a number of joints with weight J, p number of lower chord members with weight V, r number of upper chord members with weight Q, and o number of diagonal members with weight Z. The self-weight is calculated for a single bridge plane, assuming symmetry.

Constraints

The constraints, c are related to (1) limiting strains from cold bending of the flange plates, (2) transportation requirements, (3) fatigue design requirements, (4) global buckling, (5) ultimate behavior under factored load combinations, and (6) global failure mechanism. To evaluate the structural constraints, a parametric FE model was used.

Constraint c_1 limits the strains in the bent flange plates induced during cold bending by requiring that the bend radius be at least five times the thickness, consistent with bridge construction code (AASHTO, 2017a). Because both radii of curvature are 508 mm (20 in.), constraint c_1 is satisfied for every value in the set, S_T. This constraint is included for completeness.

Constraint c_2 limits the size of the joint and members to be sufficiently small for transportation in an ISO container. To achieve the stacking configuration shown in Figure 8, constraint c_2 requires that the combined height of joints and wide flange section does not exceed the internal height of the container, I. A gap [g = 12.7 mm (0.5 in.)] is assumed between each surface. The dimension w is the maximum of the depths of the s_1, s_2, and s_3 section sizes to be able to accommodate any of the members.

Constraint c_3 limits load-induced fatigue cracks in the joints. It is satisfied if the peak von Mises stress, σ, determined from linear elastic analysis, in any of the lower chord joints under the Fatigue I limit state does not exceed the nominal fatigue resistance σ_N. Thus, this constraint requires that the modular joint is classified as having an infinite fatigue life in accordance with the bridge design code (AASHTO, 2017b). Specifically, the joint falls within Category B detail (welded connections including built-up sections with fillet welds or full penetration groove welds that are loaded longitudinally), for which the nominal fatigue resistance, σ_N is 110 MPa (16 ksi).

The bridge design code Fatigue I limit state includes a single design truck positioned along the span to produce the worst effect. A dynamic load allowance of 15% is also applied to the design truck load (AASHTO, 2017b). In the FE model, the truck load is represented as point loads applied at the top flange of the floor beams and is positioned along the span to produce the worst effect.

Constraint c_4 requires that the structure does not experience instability under dead, uniform live, and wind loads with load factors of 1.25, 1.75, and 1.0, respectively, defined based on the bridge design code Strength V limit state (AASHTO, 2017b). A linear eigenvalue buckling analysis is performed to evaluate constraint c_4, in which F_D is the dead load, F_L is combined live and wind loads, ξ is the critical buckling load factor determined from the linear eigenvalue buckling analysis by applying live and wind loads on the deflected shape of the structure from dead load (determined from linear elastic analysis), and λ is the minimum acceptable critical buckling load factor (λ=1.5). The dead load includes a lightweight deck of 1.2 kN/m^2 (25 psf) as well as the self-weight of all structural steel components. The live load consists of a 18.7 kN/m (1.28 kips/ft) uniformly distributed load to represent two vehicular design lanes. The wind load consists of two design wind pressures, P_z^W = 1.57 kN/m^2 (32.8 psf) and P_z^L = 0.785 kN/m^2 (16.4 psf), respectively applied to the windward and leeward sides, with magnitudes calculated based on bridge design code (AASHTO, 2017b). In the FE model, the self-weight of the deck and the lane load are applied as a pressure along the length of each floor beam acting at the top flange of the beam. The self-weight of all members is applied through the specified density of steel and acceleration of gravity. The wind load is applied as pressure on the web of the lower chord, upper chord, diagonal members, and modular joints in both bridge planes in the transverse direction.

Constraint c_5 requires that the structure has a sufficient capacity to sustain dead and live loads with load factors of 1.25 and 1.75, respectively that are defined based on the bridge design code Strength I limit state (AASHTO, 2017b). This is quantified as requiring that at least 80% of the structure's initial elastic stiffness, K_{in} is maintained at this applied load. This is a conservative approximation of a limit state analysis, providing an estimation of the ultimate capacity of the system. The stiffness is calculated based on a load-displacement curve obtained from a linear inelastic FE analysis. Specifically, the stiffness is calculated as the slope between two successive increments in the load-displacement curve:

$$K^{h,h+1} = \frac{P_{h+1} - P_h}{\delta_{h+1} - \delta_h} \tag{16}$$

where P is the applied load, δ is the displacement of the lower chord at midspan, and h refers to the increment. The initial elastic stiffness, K_{in} is taken as the average of all stiffness values up until the end of the linear-elastic region. The end of the linear-elastic region is taken as the point where the difference between the values of two successive slopes exceeds 0.1 $\%$. The tangent stiffness, K_p is calculated using Equation 16 for every increment following this point. In the FE analyses, the dead load includes a lightweight deck of 1.25 kN/m^2 (25 psf) as well as the self-weight of all structural steel components. The live load consists of two lanes of vehicular traffic corresponding to a 18.7 kN/m (1.28 kips/ft) uniformly distributed design lane load and two design trucks, positioned to produce the worst effect. A dynamic load allowance factor of 33$\%$ is applied to the truck loads (AASHTO, 2017b). In the FE model, the loads are applied as in constraints c_3 and c_4.

Constraint c_6 relates to the failure mechanism of the structure, ensuring that the upper chord, lower chord, or diagonal members fail prior to any of the modular joints as this would be a more desirable and less catastrophic failure mechanism. It is only evaluated if constraint c_5 is satisfied, meaning that the structure maintains more than 80$\%$ of the initial elastic stiffness under the Strength I limit state. The failure mechanism is evaluated by considering the deformations of the members and the joints when the structure is progressively overloaded by increasing the uniform live load until $K_p = 80\% K_{in}$. At the node of highest deflection (node j) for the lower chord member (subscript n) and the lower chord joint (subscript m), the difference between two successive nodal rotations along the center line of the bottom flange, τ is calculated as follows:

$$\tau = |\rho_{j-1} - \rho_{j+1}| \tag{17}$$

where ρ refers to the nodal rotation and is calculated as follows:

$$\rho_{j-1} = \frac{\delta_j - \delta_{j-1}}{x_j - x_{j-1}} \tag{18}$$

$$\rho_{j+1} = \frac{\delta_j - \delta_{j+1}}{x_j - x_{j+1}} \tag{19}$$

where δ is the nodal vertical displacement and x is the nodal coordinate along the longitudinal axis.

3D Parametric Finite Element Model

To evaluate the structural constraints, a three-dimensional parametric FE model was developed in ABAQUS/Standard (ABAQUS, 2016). The model includes modular joints, chord and diagonal members, floor beams (section size W14x159), lateral bracing (section size W14x132), and portal bracing (section size W14x132). Web stiffeners [38.1 mm (1.5 in.) thick] are provided at the lower chord members, lower chord modular joints, and upper chord modular joints. Plates [25.4 mm (1 in.) thick] for connecting the lateral bracing to the upper chord are also included in the model (Figure 12).

The components are modeled with S4R or S3R (4 or 3-node reduced integration) shell elements with six degrees of freedom per node. A mesh refinement study was performed, resulting in a mesh size of 38.1 mm (1.5 in.) for the joints, both ends of the members, lateral bracing, and floor beams, where these members connect to the joints, connection plates, and stiffeners. A larger mesh size of 101.6 mm (4 in.) is used elsewhere to reduce computational expense.

The connection between members is represented through the surface-to-surface or node-to-surface tie constraints which constrain all degrees of freedom. The boundary conditions are: at one end of plane one, all translation is restrained; at the same end of plane two, free translation transversely, translation restrained in longitudinal and vertical directions; at the other end of plane one, free translation longitudinally, translation restrained in transverse and vertical directions; at the same end of plane two, free translation along the longitudinal and transverse directions, translation restrained in vertical direction. Free rotation about the longitudinal, transverse and vertical axes is allowed at all locations. The boundary conditions are applied at the middle of the bottom flange of each of the end joints. For all members, Grade 50 structural steel with specified minimum yield strength 345 MPa (50 ksi), modulus of elasticity 200 GPa (29000 ksi), steel density of 7850 kg/m^3 (490 lbs/ft^3), and Poisson's ratio 0.3 is used. For the linear inelastic analysis, a non-linear material model was developed by prescribing an elastic-perfectly plastic stress-strain relationship.

Algorithms

The optimization problem (Equation 15) is solved using the stochastic algorithms Simulated Annealing (SA) and Descent Local Search (DLS) that search the design space, as the design variables are discrete and the constraints are nonlinear.

SA was first proposed by Kirkpatrick et al. (1983) and has been widely used in structural optimization applications (e.g., Paya et al., 2008; Thrall et al., 2012, 2014; Russell et al., 2014). The method is based on an analogy to the process of forming crystals through heating and slow cooling of a material. At high temperatures, the atoms are able to move randomly, forming new configurations with primarily lower internal energy. However, a certain probability exists that states with higher energy are formed, ultimately allowing the atoms to reach a state with lower energy. This probability, P_r is given by: $P_r = exp(- \triangle E/T)$, where $\triangle E$ is the difference in energy between two configurations and T is the temperature. As the temperature is decreased, the probability of forming states with higher energy also decreases (Arora, 2004; Arora et al., 1994). Based on this concept, Kirkpatrick et al. (1983) introduced an iterative approach to solving optimization problems, where E is related to the objective function, P_r is related to the probability that solutions with a higher value of the objective function are accepted, and T is a parameter that is initially defined and can be controlled. The probability of accepting solutions with higher value objective function allows the algorithm to escape local minima.

The SA algorithm implemented in this research begins by selecting the highest value in the discrete sets S_T and S_B as the initial vector of design variables. This ensures an initial solution that is feasible. This initial solution is both the current (i.e., the solution upon which the algorithm is iterating on) and the best solution (i.e., lowest value of the objective function solution). The algorithm then finds a new solution by randomly perturbing the design variables along the length of the discrete set of design variables, S_T or S_B. The number of variables to be varied are randomly selected from 1 to v, where v is a user-defined parameter. The variable(s) to be varied are randomly selected. The variables are perturbed by a random amount up to a user-defined parameter, pm. The direction, up or down the set (S_T and S_B are in ascending order), is randomly selected. The new solution is then evaluated. If the new solution is feasible and the new weight is less than the current weight, the solution is accepted as the current solution. It is also the best solution. If the solution is feasible, but the weight is higher than the current solution, the algorithm calculates the probability of accepting the higher-weight solution as the current solution. If it is not accepted, the solution is rejected and the current solution is maintained. The algorithm continues for a user-defined number of iterations, m which forms one cycle. For each cycle, T is kept constant. For the first cycle, an initial value for T is chosen such that the acceptance of higher value objective functions is between 20% and 40% (Medina, 2001). Due to the huge computational expense to run all structural analyses, the initial T is found without evaluating any of the structural constraints (c_3 to c_6). When all iterations within a cycle are finished, the temperature is reduced by a user-defined parameter, rt and a new cycle begins. The reduction of T decreases the probability of accepting higher value solutions. The algorithm converges when for a predefined number of cycles, n the best solution has not been updated.

The DLS algorithm is similar to SA, but without the probability of accepting higher objective function value solutions. Convergence is defined as a certain number of iterations, it for which the objective function has not been decreased. The best solution is the last feasible solution.

Results

The results from several tests using the SA and DLS algorithms, including the average solution weight, μ, standard deviation, σ, coefficient of variation, C_v, lowest weight, W_{min}, and corresponding design variables, $\mathbf{t}$ and $\mathbf{s}$ are presented in Table 2. Both SA and DLS algorithms result in nearly equivalent lowest weight solutions [SA-1 and SA-2 with 1201 kN (270 kips) and DLS-1 with 1208 kN (272 kips)]. Although, SA finds the lowest weight solution, the lower coefficient of variation for DLS-1 indicates better convergence among the ten tests. The convergence curve of the lowest weight solution for both algorithms is presented in Figure 13. The capability of SA to escape local minimum is clearly shown by the fluctuations in Figure 13A. However, both curves follow a similar trend and ultimately converge to almost the same weight. This shows that both algorithms are suitable for the optimization problem. However, comparing the time to run the optimization, DLS is able to achieve convergence more rapidly than SA. This is particularly noticeable when the numbers of cycles, n are increased as in SA-2 which resulted in a significantly higher run time compared to the other cases.

The lowest weight solution of W_{min} = 1201 kN (270 kips), which is found through both SA-1 and SA-2, results in an optimized design of the modular joints and members. The algorithm has selected member section sizes primarily to satisfy the global buckling and failure constraints (c_4 and c_6). Due to bending of the lower chord and peak tensile forces at midspan, the lower chord members are W14x233 wide flange sections that have high in-plane stiffness. Similarly, to provide enough compressive capacity in the upper chord and prevent member buckling, the algorithm has selected W14x193 wide flange sections which have a considerable out-of-plane stiffness. Because the diagonal members have very small (close to zero) forces, the algorithm has selected the wide flange section W14x109 which is the smallest in the given database. The modular joint design variables are similarly selected based primarily on the structural constraints. Due to high axial forces in the chords, the thickness of the bent flange plate, t_1 is 50.8 mm (2 in.) which is close to the limit value of 63.5 mm (2.5 in.). This is because a large cross sectional area is required to transfer the chord axial forces from the bent flange to the web zone. The thickness t_3 = 34.9 mm (1.375 in.) has a lower value compared to t_1 which is primarily because the flange is a straight plate and provides a continuous load path of the chords axial forces. The small forces in the diagonal members result in a thickness t_2 = 12.7 mm (0.5 in.), the smallest value in the database. The algorithm, however, selects a relatively thick web plate, t_4 = 44.5 mm (1.75 in.). The thick web provides a way to handle the stress concentration within the web zone. Furthermore, a thicker web plate is beneficial for the global stability of the structure as it increases its out-of-plane stiffness.

The response of the lowest weight solution is presented in Figure 14. The load-displacement curve (Figure 14A) developed from a linear inelastic analysis indicates that the structure's response under Strength I limit state (constraint c_5) is primarily in the linear elastic range which is desirable. The structure can sustain loads up to 12,035 kN while keeping more than 80$\%$ of its initial stiffness. As the bridge is overloaded (increased uniform live load), the initial elastic stiffness is reduced which is indicated in the load-displacement curve by a slight plateau range followed by a positive slope. At a load of 12,268 kN, the tangent stiffness, K_p is 80$\% K_{in}$. The structure has developed excessive deformations and, as clearly shown in Figure 14B, the wide flange member in the lower chord at midspan has failed. Figure 14C shows the buckling mode shape of the structure corresponding to the critical load factor ξ = 3.9 which is bigger than the minimum acceptable buckling load factor λ = 1.5. The structure experiences local out-of-plane buckling at midspan where the compressive force is the highest which is also a desirable and expected mode shape.

CONCLUSIONS

This paper presented a modular joint as a new approach for the accelerated fabrication and erection of steel bridges. It is a kit-of-parts comprised of (1) a single prefabricated modular joint, (2) standard wide flange sections, and (3) bolted splice connections, that can be used for a wide range of spans and loadings. The modular joint provides significant structural advantages including: (1) the use of splice connections in double shear increases the efficiency and decreases construction time and cost by reducing the number of bolts, (2) the splices are located to facilitate inspection, maintenance, and repair, and (3) the strong axis orientation of the members and moment-resisting connections between the members results in increased flexural capacity, providing the potential for the chords to carry load in bending if a diagonal is lost. The modular joint, in comparison with the existing modular systems, can achieve greater spans, while providing capabilities for shorter spans.

This paper proposed methodologies for achieving rational-form bridges. More specifically, a family of constant-depth simply supported bridges with different span lengths was introduced. By requiring the same span-to-depth ratio as well as the same number of modular joints to be used for each bridge in the family, the methodology achieves the desired spans using the kit-of-parts and changing only the length of wide flange members. This research also introduced a methodology for achieving rational form variable-depth bridges. By connecting the joints and members at angles, the depth of the structure can vary, allowing more efficient bridge forms to be developed.

A sizing optimization approach to minimize the self-weight of structures comprised of the modular joint and wide flange members was proposed. The optimization was implemented for the case study of a 119-m (390-ft) constant-depth simply supported bridge. To ensure transportability and sufficient structural capacity, geometric and structural constraints were considered. The optimization problem was solved using two stochastic search algorithms: SA and DLS. Results show that DLS and SA are suitable for this optimization problem as both algorithms resulted in nearly equivalent lowest weight solution. The promise of the modular joint is clearly demonstrated through the structural behavior of the lowest weight solution found by the SA algorithm.

Ultimately this paper presents a new approach to modular construction in which the joint becomes the module that is used to achieve a wide range of bridges.

This research has focused on the behavior of the system under service and ultimate loads. Future research should investigate erection strategies and the behavior of the system during erection. Erection strategies such as launching or balanced cantilever are appealing as they do not require as much heavy lifting equipment as conventional truss construction. These techniques cannot typically be used for trusses as conventional gusset plates cannot transmit flexure. The unique characteristic of the modular joints being able to carry flexure opens up these alternative and efficient construction strategies. As in the construction of conventional bridges, careful erection analysis must be performed to control the geometry. Fit-up of the connections should also be considered in the erection engineering. The components could be fabricated for either no load fit or steel dead load fit. To promote modularity and a one-size-fits-all approach, no load fit is an appealing strategy as the modular joints could be fabricated identically, regardless of application. Force-fitting would be required in the field, but the splice connections between components could be readily used to achieve the necessary changes to geometry. Camber and geometry control during erection can also be incorporated through the bent flange splice connections between the modular joints and members.

DATA AVAILABILITY STATEMENT

All data, models, or code that support the findings of this study are available from the corresponding author upon reasonable request.

ACKNOWLEDGMENTS

This material is based upon work supported by the National Science Foundation under Grant No. CMMI-1351272. Mirela D. Tumbeva is also supported by the O.H. Ammann Research Fellowship. Support from these sources and the program managers is gratefully acknowledged.

REFERENCES

AASHTO (2017a). *AASHTO LRFD Bridge Construction Specifications*. American Association of State Highway and Transportation Officials (AASHTO), Washington, D.C., 4th edition.

AASHTO (2017b). *AASHTO LRFD Bridge Design Specifications, Customary U.S. Units*. American Association of State Highway and Transportation Officials (AASHTO), Washington, D.C., 8th edition.

ABAQUS (2016). *ABAQUS/Standard Analysis User's Manual Version 6.14*. Dassault Systemes, Waltham, MA.

AISC (2011). *Steel Construction Manual*. American Institute of Steel Construction (AISC), Chicago, IL, 14th edition.

Arora, J. S. (2004). *Introduction to Optimum Design*. Elsevier Academic Press, San Diego, CA, 2nd edition.

Arora, J. S., Huang, M. W., and Hsieh, C. C. (1994). "Methods for optimization of nonlinear problems with discrete variables: a review." *Structural Optimization*, 8(2), 69–85.

Bell, E. S. and Medina, R. A. (2019). "Evaluation of gusset-less truss connection to aid bridge inspection and condition assessment." *Technical Report No. FHWA-NH-RD-26962M*.

Chen, J. G., Adams, T. M., Sun, H., Bell, E. S., and Büyüköztürk, O. (2018). "Camera-based vibration measurement of the World War I Memorial Bridge in Portsmouth, New Hampshire." *Journal of Structural Engineering*, 144(11), 04018207.

Covington, E., Engel, C., Kelly-Sneed, K., Noh, J., and Zoli, T. P. (2013). "Portsmouth Memorial Bridge replacement: An exploration of truss design without gusset plates." *Proceedings of the 2013 SEI Illinois Chapter Lecture Series*.

Department of the Army (1986). "Bailey bridge." *Field Manual No. 5-277*, Headquarters, Department of the Army, Washington, DC.

Gerbo, E. J., Casias, C. M., Thrall, A. P., and Zoli, T. P. (2016a). "New bridge forms composed of modular bridge panels." *Journal of Bridge Engineering*, 21(4), 04015084.

Gerbo, E. J., Thrall, A. P., Smith, B. J., and Zoli, T. P. (2016b). "Full-field measurement of residual strains in cold bent steel plates." *Journal of Constructional Steel Research*, 127, 187–203.

Gerbo, E. J., Thrall, A. P., and Zoli, T. P. (2020a). "Adjustable bolted steel plate connection: measured behavior of bolts during field installation and numerical parametric investigation." *Journal of Structural Engineering*, 146(2), 04019189.

Gerbo, E. J., Thrall, A. P., and Zoli, T. P. (2020b). "Service and ultimate behavior of adjustable bolted steel plate connections." *Journal of Structural Engineering*, 146(7), 04020128.

Gerbo, E. J., Wang, Y., Tumbeva, M. D., Thrall, A. P., Smith, B. J., and Zoli, T. P. (2018). "Behavior of an adjustable bolted steel plate connection during field installation." *Journal of Structural Engineering*, 144(3), 04017223.

Gerbo, E. J., Wang, Y., Tumbeva, M. D., Thrall, A. P., Smith, B. J., and Zoli, T. P. (2019). "Closure to 'Behavior of an Adjustable Bolted Steel Plate Connection during Field Installation' by Evan

J. Gerbo, Yao Wang, Mirela D. Tumbeva, Ashley P. Thrall, Brian J. Smith, and Theodore P. Zoli." *Journal of Structural Engineering*, 145(3), 07018015.

ISO (2013). *ISO 668: Series 1 freight containers - Classification, dimensions, ratings.* ISO, Switzerland, 6th edition.

Joiner, J. H. (2001). *One More River to Cross: The Story of British Military Bridging*. Pen and Sword Books Ltd, South Yorkshire, UK.

Keating, P. B. and Christian, L. C. (2012). "Effects of bending and heat on the ductility and fracture toughness of flange plate." *Technical Report No. FHWA/TX-10/0-4624-2*.

Kirkpatrick, S., Gelatt, C. D., and Vecchi, M. P. (1983). "Optimization by simulated annealing." *Science, New Series*, 220(4598), 671–680.

Mashayekhi, M. and Santini-Bell, E. (2019). "Fatigue assessment of the gusset-less connection using field data and numerical model." *Bridge Structures*, 15(1-2), 75–86.

Medina, J. R. (2001). "Estimation of incident and reflected waves using simulated annealing." *Journal of Waterway, Port, Coastal, and Ocean Engineering*, 127(4), 213–221.

Paya, I., Yepes, V., Gonzalez-Vidosa, F., and Hospitaler, A. (2008). "Mutliobjective optimization of concrete frames by simulated annealing." *Computer-Aided Civil and Infrastructure Engineering*, 23, 596–610.

Russell, B. R. and Thrall, A. P. (2013). "Portable and rapidly deployable bridges: Historical perspective and recent technology developments." *Journal of Bridge Engineering*, 18(10), 1074–1085.

Russell, B. R., Thrall, A. P., Padula, J. A., and Fowler, J. E. (2014). "Reconceptualization and optimization of a rapidly deployable floating causeway." *Journal of Bridge Engineering*, 19(4), 04013013.

Shahsavari, V., Mashayekhi, M., Mehrkash, M., and Santini-Bell, E. (2019). "Diagnostic testing of a vertical lift truss bridge for model verification and decision-making support." *Frontiers in Built Environment*, 5(92), 1–19.

Thrall, A. P., Adriaenssens, S., Paya-Zaforteza, I., and Zoli, T. P. (2012). "Linkage-based movable bridges: Design methodology and three novel forms." *Engineering Structures*, 37, 214–223.

Thrall, A. P., Zhu, M., Guest, J. K., Paya-Zaforteza, I., and Adriaenssens, S. (2014). "Structural optimization of deploying structures composed of linkages." *Journal of Computing in Civil Engineering*, 28(3), 04014010.

Wang, Y. T., P., A., and Zoli, T. P. (2016). "Adjustable module for variable depth steel arch bridges." *Journal of Constructional Steel Research*, 126, 163–173.

List of Tables

TABLE 1. Definition of angles γ between modular joint and wide flange members.

Angle notation	Position	Value
γ_i^1	Between M_i and L_{i-1} at point C	Varied within given range
γ_i^2	Between T_{i-1} and U_i at point A'	Varied within given range
γ_i^3	Between N_i and U_i at point B	$\gamma_i^6 - \gamma_i^1 + \gamma_i^5$
γ_i^4	Between T_i and U_i at point A	Varied within given range
γ_i^5	Between M_i and U_i at point B'	$\gamma_i^1 - \alpha_i$
γ_i^6	Between N_i and L_i at point C'	$\arctan\left(\frac{y_{U_i}-(l/2)[\sin\theta+\sin(\theta+\alpha_i)]}{x_{L_i}-x_{U_i}-(l/2)[\cos\theta+\cos(\theta+\alpha_i)]}\right) - \theta$

TABLE 2. Optimization results.

Test	N tests	n (for SA), it (for DLS)	Other Parameters	Results			Lowest weight results								
				μ	σ	C_v	W_{min}	t_1	t_2	t_3	t_4	s_1	s_2	s_3	Run time
				(kN)	(kN)	%	(kN)	(mm)	(mm)	(mm)	(mm)	W14x	Wx14	Wx14	(min)
SA-1	10	1	v=1, pm=5, m=50, rt=0.8	1240	43.1	3.48	1201	50.8	12.7	34.9	44.5	233	193	109	9873
SA-2	10	2		1225	18.4	1.51	1201	50.8	12.7	34.9	44.5	233	193	109	13019
DLS-1	10	100	v=1, pm=5	1226	12.1	0.99	1208	50.8	12.7	31.8	47.6	233	193	109	6623
DLS-2	10	200		1233	10.2	0.83	1218	41.3	12.7	34.9	44.5	257	193	109	8446

List of Figures

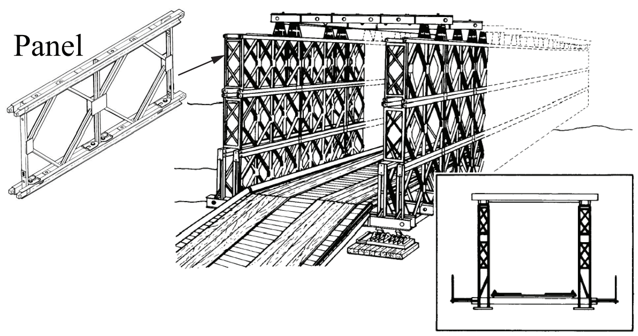

FIG. 1. Example of the state-of-the-art in modular bridges. Reprinted from Department of the Army (1986).

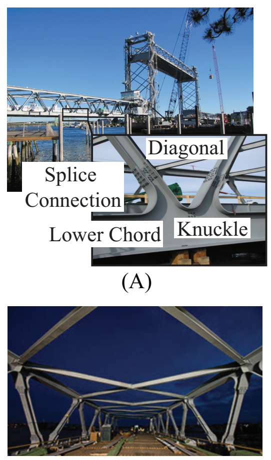

(A)

(B)

FIG. 2. Memorial Bridge connecting Portsmouth, NH and Kittery, ME: (A) Photograph of the knuckle and (B) Photograph from the deck. Image courtesy of HNTB Corporation.

(A) (B)

FIG. 3. Fabrication of Memorial Bridge: (A) Cold bending of flange plates and (B) Welding of flange plate to web plate. Image courtesy of HNTB Corporation.

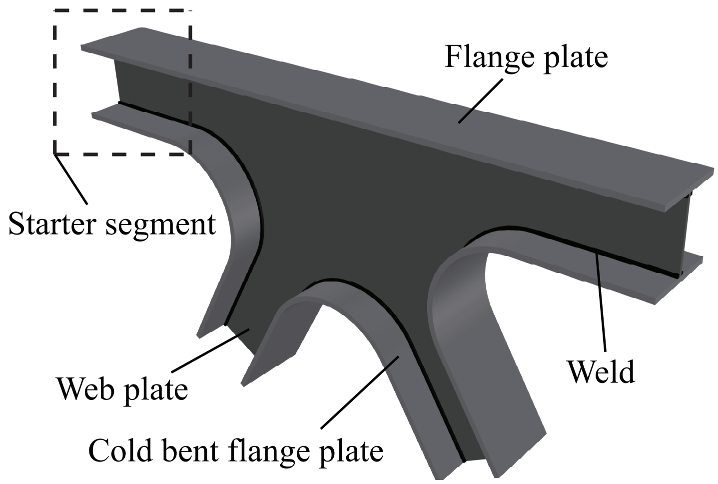

FIG. 4. Modular joint.

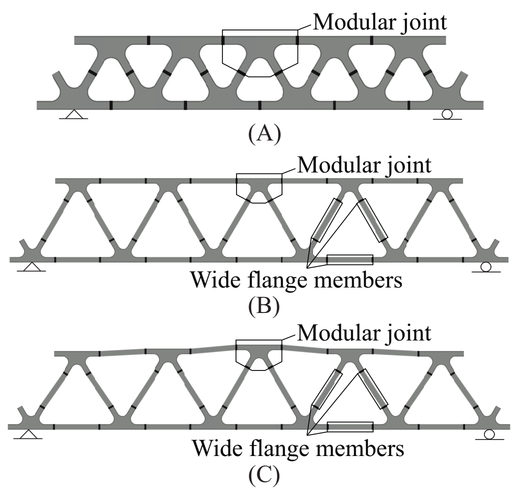

FIG. 5. Modular approach to: (A) Short-span constant-depth bridge, (B) Long-span constant-depth bridge, and (C) Long-span variable-depth bridge.

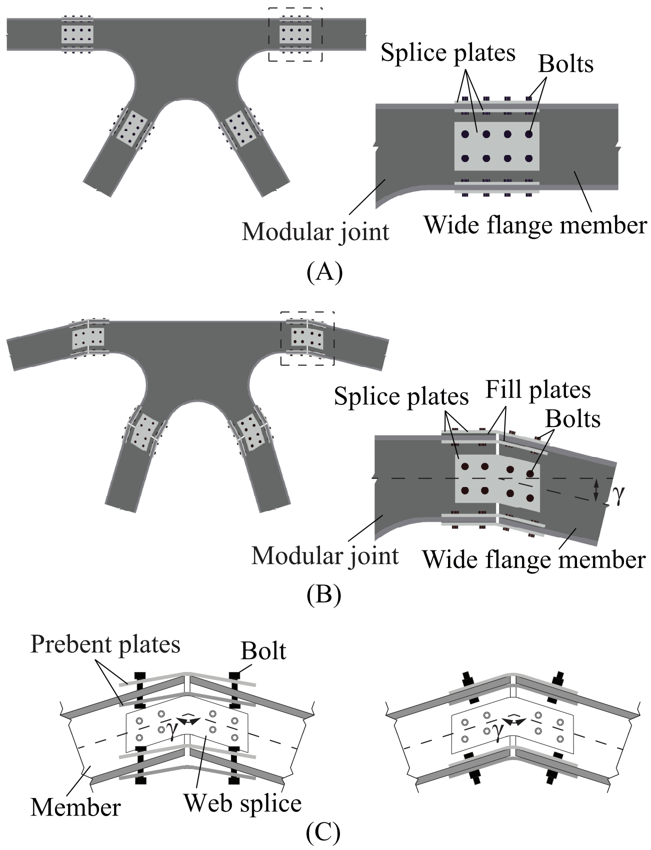

FIG. 6. Connection between modular joints and members: (A) Via straight splice plates, (B) Via adjustable bolted steel plate connection, and (C) Field installation of the adjustable steel plate connection by bolt tightening: untightened (left) and final tightened (right) state [(C) adapted from Gerbo et al. (2019, 2020a), ©ASCE].

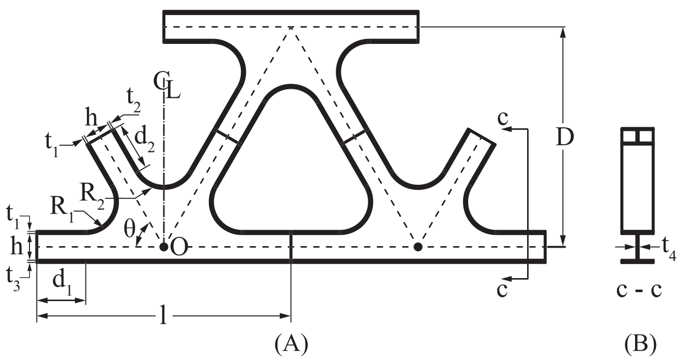

FIG. 7. Geometric development of the modular joint: (A) Elevation view of back-to-back modular joints and (B) Section view of one modular joint.

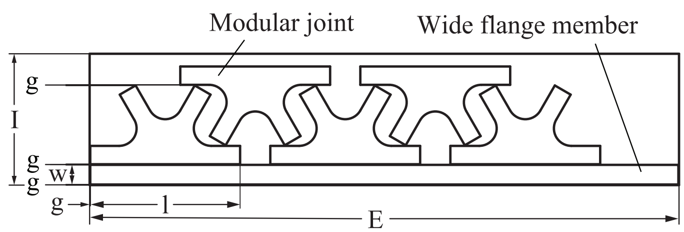

FIG. 8. Elevation view of modular joints and wide flange section stacked vertically within the foot print of an ISO container.

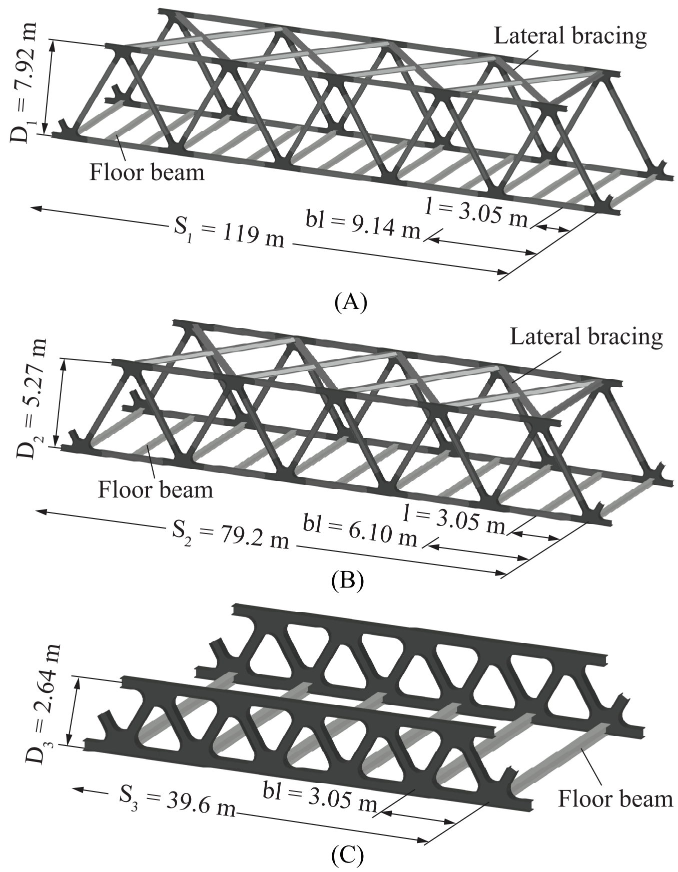

FIG. 9. Isometric view of family of constant-depth simply supported bridges: (A) 119-m span (b=3), (B) 79.2-m span (b=2), and (C) 39.6-m span ($b = 1$).

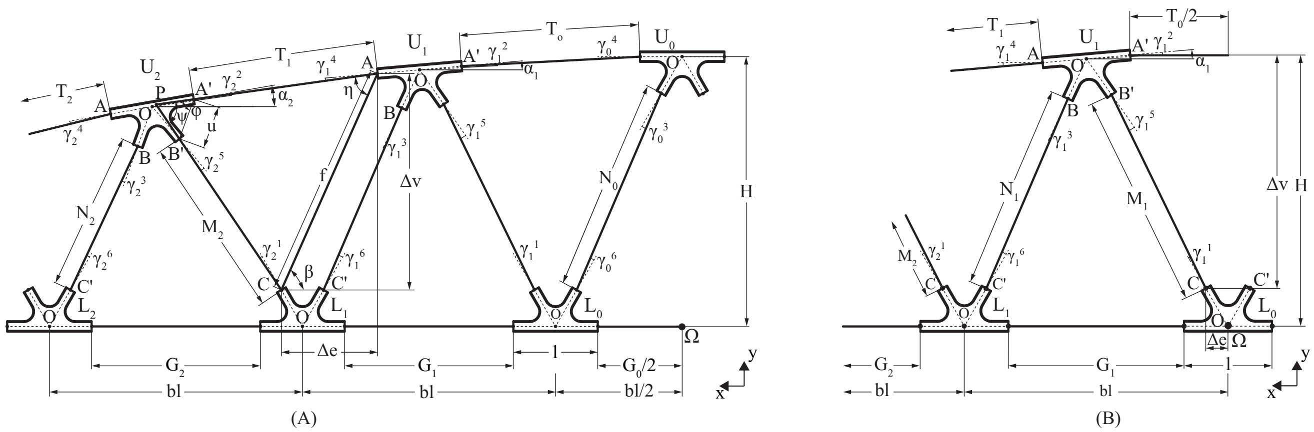

FIG. 10. Geometric development of variable-depth bridges: (A) Simply supported bridge and (B) Three-span continuous bridge, angles γ given in Table 1.

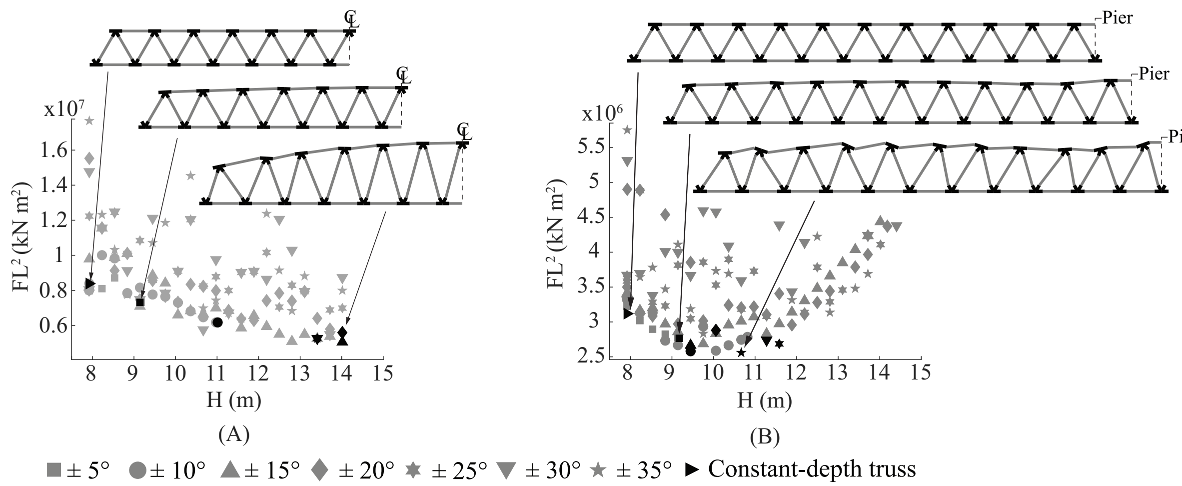

FIG. 11. Form-finding results for variable-depth bridges: (A) Simply supported bridge and (B) Three-span continuous bridge. Black marks denotes the lowest metric FL^2 for each γ_{max}.

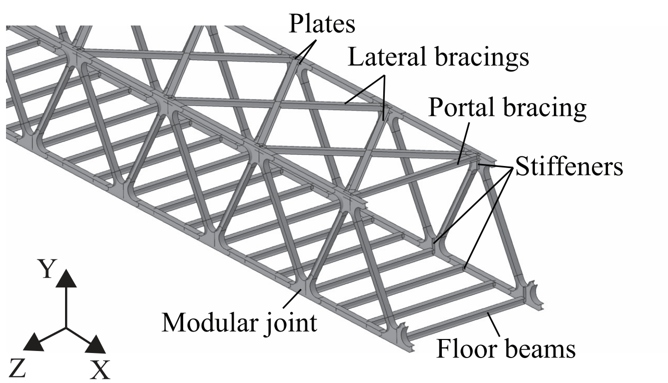

FIG. 12. Parametric finite element model.

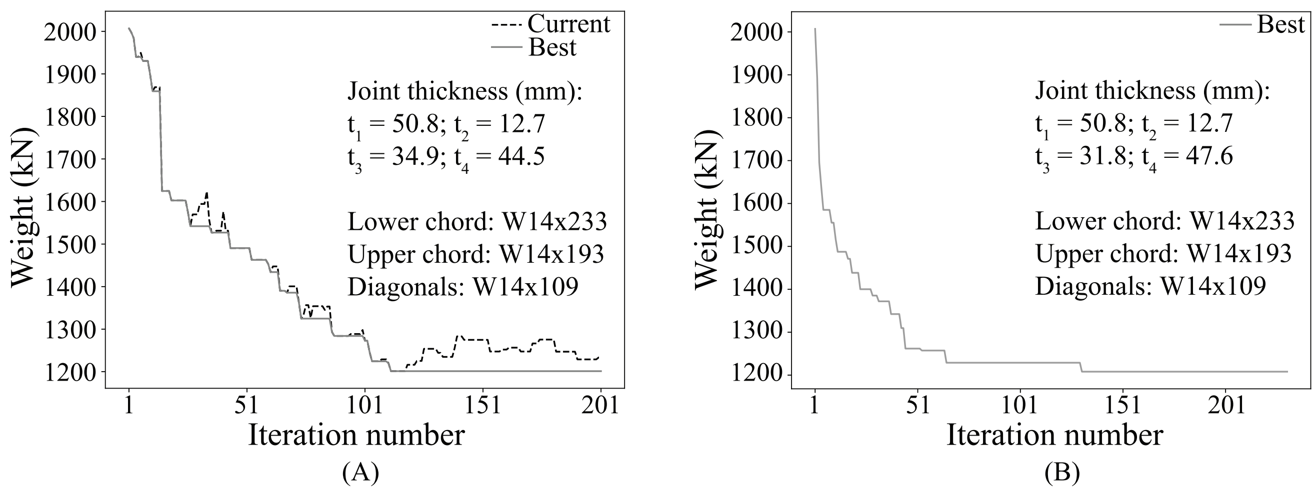

FIG. 13. Convergence curves for the lowest weight solution: (A) SA algorithm, and (B) DLS algorithm.

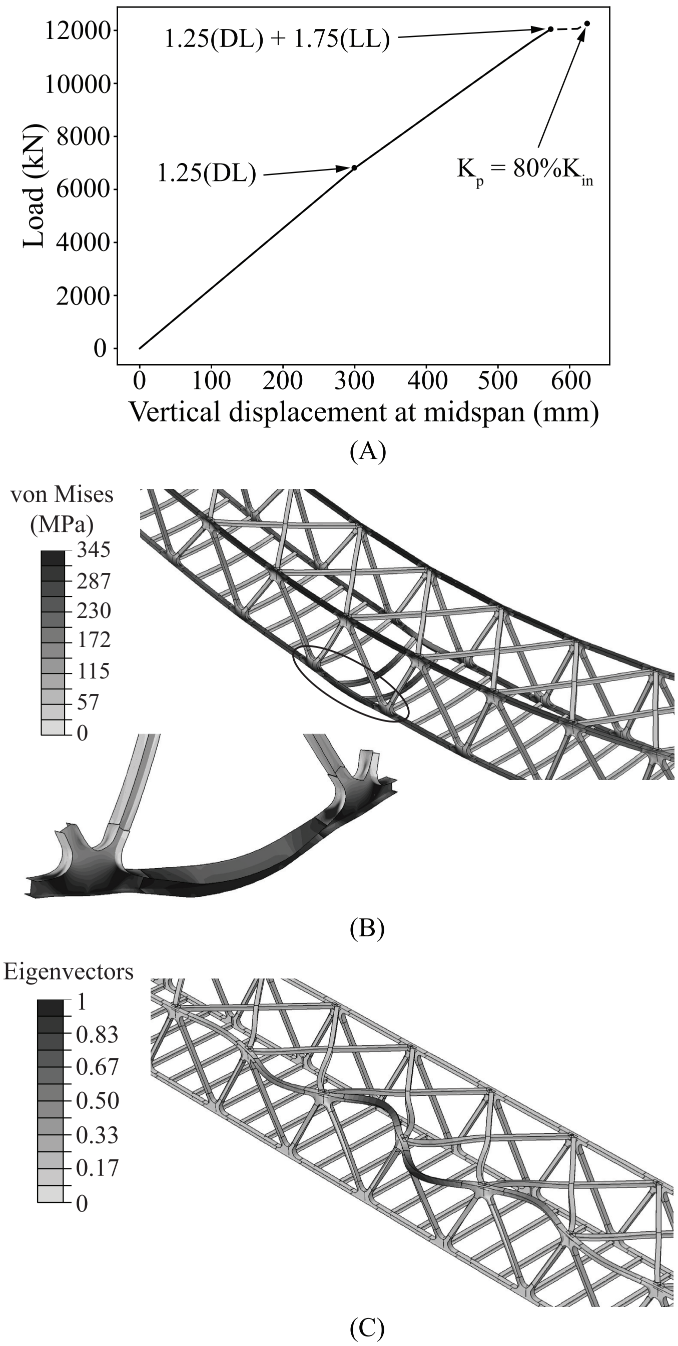

FIG. 14. Response of the structure with the lowest weight solution: (A) Load-displacement curve from linear inelastic analysis (DL = dead load, LL = live load), (B) Failure mechanism described by von Mises stress contour at midspan, and (C) Buckling mode shape corresponding to the critical load factor (smallest eigenvalue) of 3.9.